ACS OMEGA

Article

Cite This: ACS Omega 2018, 3, 8111−8121

Nanocrystalline Cellulose-Derived Doped Carbonaceous Material for Rapid Mineralization of Nitrophenols under Visible Light

Ambar B. RanguMagar,[†] Bijay P. Chhetri,[†] Anil Parameswaran-Thankam,[†] Fumiya Watanabe,[‡] Arvind Sinha,[§,∥] Jin-Woo Kim,[§,∥] Viney Saini,[‡] Alexandru S. Biris,[‡] and Anindya Ghosh*[,†]

[†]Department of Chemistry and [‡]Center for Integrative Nanotechnology Sciences, University of Arkansas at Little Rock, 2801 South University Avenue, Little Rock, Arkansas 72204, United States

[§]Department of Biological & Agricultural Engineering and [∥]Institute for Nanoscience and Engineering, University of Arkansas, Fayetteville, Arkansas 72701, United States

Supporting Information

ABSTRACT: Nitrophenols (NPs) and related derivatives are industrially important chemicals, used notably to synthesize pharmaceuticals, insecticides, herbicides, and pesticides. However, NPs and their metabolites are highly toxic and mutagenic. They pose a serious threat to human health and ecosystem. Current work was undertaken to develop a suitable visible-light active catalyst for the sustainable and efficient mineralization of NPs in an aqueous environment. Nanocrystalline cellulose (NCs)-based nitrogen-doped titanium dioxide and carbonaceous material (N-TiO_2/C) was synthesized by pyrolysis and sol−gel methods using NCs, polydopamine, and TiO_2. The synthesized N-TiO_2/C was characterized using different analytical techniques. Photocatalytic degradation of NPs under visible light indicated that acidic pH (3) was most suitable for the optimal degradation. 4-NP degradation followed both pseudo-first-order (R^2 = 0.9985) and Langmuir−Hinshelwood adsorption kinetic models (adsorption constant, K_{LH} = 1.13 L mg^{-1}). Gas chromatography−mass spectrometry and ion chromatography analysis confirmed the total mineralization of 4-NP into smaller molecular fragments such as acids, alcohols, and nitrates. The total organic carbon showed that 67% of total carbon present in 4-NP was mineralized into CO_2 and CO. The catalyst was recycled for five consecutive cycles without losing its catalytic activities. The degradation mechanism of NPs with N-TiO_2/C was also explored.

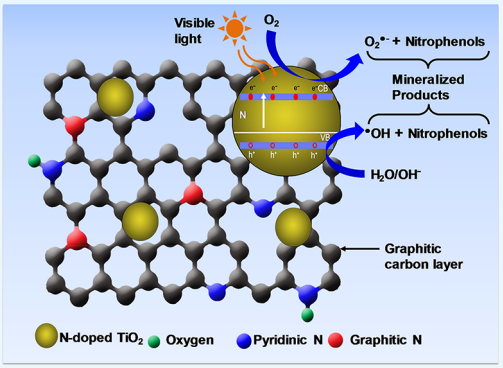

INTRODUCTION

Water pollution has become a global issue in today's world. Modern societies and industries are responsible for the utilization and subsequent release of hazardous chemicals such as heavy metals, organic halogens, dyes, nitroaromatic compounds, and so forth into the environment.[1] Among them, nitrophenols (NPs) and their derivatives have been detected in water and atmosphere in significant levels.[2] Inappropriate waste disposal practice, medical, agricultural, and industrial uses are the causes for NP contamination in water. Microbial degradation or photodegradation of industrial products such as pesticides, synthetic dyes, and pharmaceuticals (Figure 1a) enables the NPs to be released into the atmosphere.[3,4] Thus, NPs are found in all places and humans are most likely to get exposed to environmental NPs through breathing, drinking, eating, and skin contact.[5] Human exposure to NPs causes eye and skin irritation and damage of functionally important organelles such as kidney, liver, central nervous system, and so forth.[6,7] The U.S. Environmental Protection Agency (EPA) has listed 4-NP as one of the "priority environmental pollutants" because of its toxicity, carcinogenic, and mutagenic effects.[8] According to the EPA report, the maximum permissible concentration of 4-NP in water is restricted to be <10 ng L^{-1}. This impels researchers to develop some new techniques where complete removal of NPs could be achievable. Over the several decades, a variety of techniques such as adsorption, biodegradation, chemical oxidation, and so forth have been identified for the NP decontamination. However, they are always associated with some sorts of disadvantages.[9−11] For example, the adsorption process is insufficient to provide complete decontamination of NPs. It simply transforms NPs into the other secondary forms. On the other hand, the chemical partial oxidation process may generate intermediates of NPs which are more toxic than the original compound. Therefore, developing a new remediation method which can remove NPs completely and economically is an attractive area of research in wastewater treatment.

Recently, photocatalytic treatment of NPs using TiO_2 has gained a lot of attention. TiO_2 have several advantages such as high thermal and chemical stability, low cost, and non-toxicity.[12] TiO_2-based nanomaterials are highly photoactive and result in complete mineralization of the pollutants.[13,14]

Received: May 16, 2018
Accepted: July 5, 2018
Published: July 19, 2018

DOI: 10.1021/acsomega.8b01020
ACS Omega 2018, 3, 8111−8121

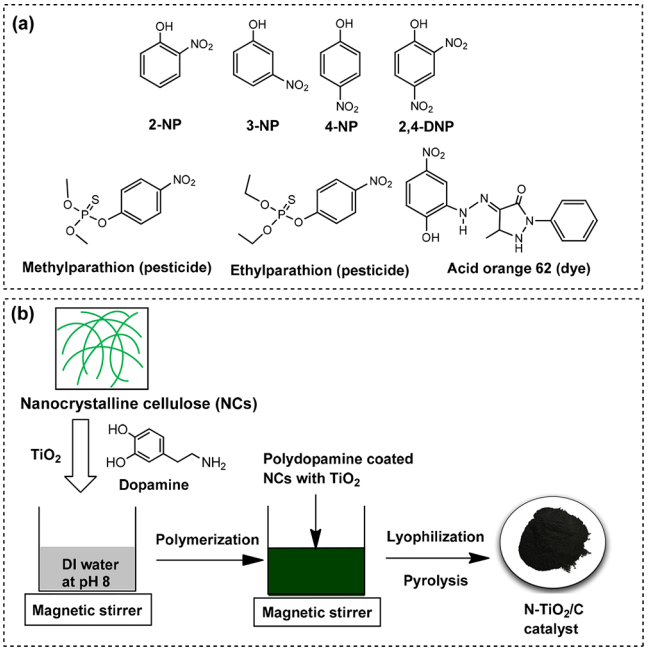

Figure 1. Schematic diagram of (a) structures of different NPs and NP-containing organic pollutants and (b) synthesis of the N-TiO_2/C catalyst.

However, because of the large band gap (~3.3 eV), TiO_2 requires high energy ultraviolet (UV) light for the photocatalytic activation.[15] This limits the practical and large scale application of TiO_2 as a photocatalyst material for effective remediation of NPs from the environment. An effort has been made to extend the light absorption of TiO_2 in the visible light region making it more economical and safe.[16] Dye sensitization, ion-implantation, and doping of metal atoms or ions have been applied to increase the optical response of the TiO_2 catalyst.[15] These methods have been found to be effective in retarding the rate of the e−h recombination and increasing the overall lifetime of photoinduced oxidation and reduction process.[16] Metal-doped TiO_2 photocatalysis is quite popular but major drawbacks are the high cost, toxicity of metals, and photocorossion.[17] One of the most feasible ways to enhance visible light photocatalytic activity of TiO_2 is heteroatom doping, such as nitrogen (N).[18] This method obviates the use of expensive and toxic metals. N-doping improves the charge transfer process by introducing a large electron donor state near the Fermi level of TiO_2.[3] Furthermore, TiO_2 with different nanostructures such as a nanotubes, nanospheres, and nanowires are possible also through N-doping.[19] As a result, N-doped TiO_2 possesses unique optical and electronic properties than bulk TiO_2 and improves the overall photocatalytic activity toward degradation of pollutants. To further enhance the catalytic activity of N-doped TiO_2, carbonaceous nanomaterials are useful because of their high specific surface area, improved thermal and electrical conductivity, porosity, and mechanical strength.[19,20] Because of these characteristics properties, they help in enhancing the loading capacity of catalysts, lowering the aggregation, and increasing the chances of separation and recovery of catalysts for consecutive uses.[21] So far, carbon nanotubes,[22] graphene,[23] and reduced graphene oxide[24] have been used to generate various types of N-doped TiO_2 nanocomposites. However, because of probable inherent nanotoxicity, their use for

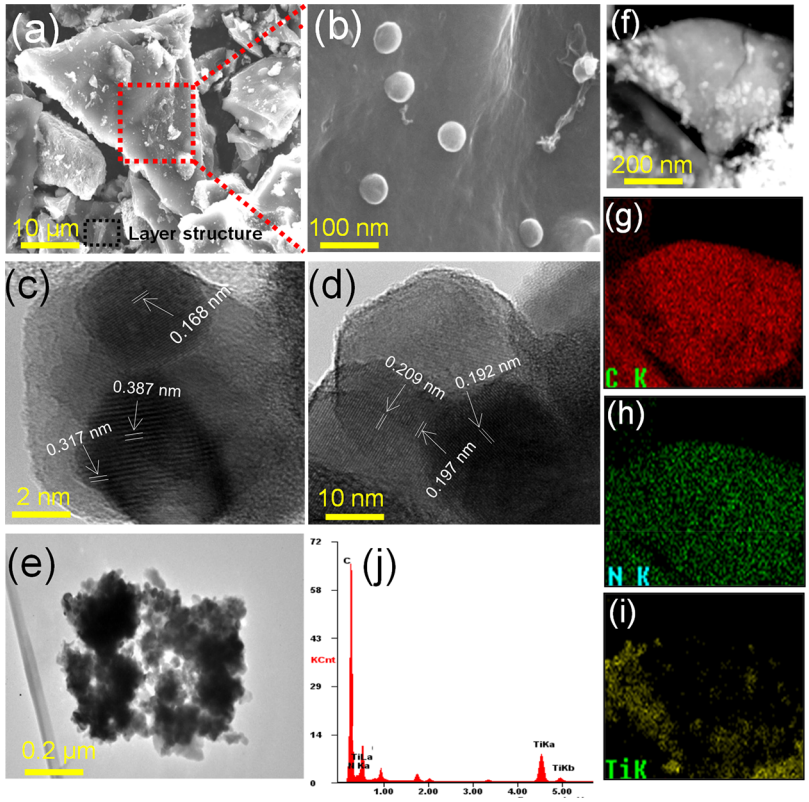

Figure 2. SEM images (a) ×2000 and (b) ×100 000 magnifications, TEM images (c−e), EDAX spectra (j), STEM image (f), and corresponding elemental mapping images for carbon (g), nitrogen (h), and titanium (i) of N-TiO_2/C.

DOI: 10.1021/acsomega.8b01020
ACS Omega 2018, 3, 8111−8121

sustainable and environment-friendly processes appear to be limited. In this context, nanocrystalline cellulose (NCs) seems to be a promising candidate.

NCs is a new class of nanomaterial derived from cellulose, which is a naturally abundant, biodegradable, biocompatible, and renewable source.[25,26] NCs have garnered much attention in recent years owing to its unique physicochemical properties and myriad applications.[27,28] NCs possess high specific surface area, high crystallinity, superior mechanical strength, and tunable chemistry.[26] These properties make NCs a fascinating material for various applications.[29] However, limited work has been done on NCs for making carbonaceous material-doped metal nanocomposites.[27] The aim of the present investigation is to exploit the unique physicochemical property of NCs for developing a sustainable and efficient, visible light active N-doped TiO_2 and carbon nanocomposites catalyst (N-TiO_2/C). For the synthesis of our catalyst (N-TiO_2/C), NCs and dopamine were selected as a source of carbon and N dopant, respectively. Dopamine undergoes self-polymerization in alkaline pH in the open air to form polydopamine, a bioinspired polymer, which forms a strong coating on any surface easily.[30] Therefore, when TiO_2 and NCs were mixed in the presence of dopamine under alkaline condition, polydopamine forms in situ and it helps to immobilize TiO_2 on the NCs.[31] Furthermore, when mixed together TiO_2 alone is capable of forming weak co-ordinate covalent bond with the hydroxyl (−OH) groups present in NCs. However, in the presence of polydopamine, TiO_2 is immobilized strongly to the surfaces of NCs. Therefore, such a design may furnish better N-doping to both TiO_2 and carbonaceous material. Finally, the synthesis of desired N-TiO_2/C photocatalyst was achieved by the pyrolysis of a lyophilized sample containing polydopamine-immobilized TiO_2 on NCs. The structure morphology, chemical composition, and elemental mapping of N-TiO_2/C were analyzed by scanning electron microscopy (SEM), Brunauer−Emmett−Teller analysis (BET), transmission electron microscopy (TEM), energy dispersive X-ray analysis (EDAX), thermal gravimetric analysis (TGA), Fourier transform infrared (FT-IR) spectroscopy, and X-ray photoelectron spectroscopy (XPS). The photocatalytic activity of N-TiO_2/C on NPs degradation was studied using both UV and visible light sources. We demonstrated that N-TiO_2/C showed excellent reactivity in NP degradation under visible light. To the best of our knowledge, this is the first report of synthesis, characterization, and applications of N-TiO_2/C which was produced using NCs, dopamine, and TiO_2.

RESULTS AND DISCUSSION

The morphology of the N-TiO_2/C was observed by SEM and TEM analysis (Figure 2). Figure 2a,b shows the SEM images of N-TiO_2/C at different magnifications. As shown in Figure 2a, it can be observed that the N-TiO_2/C surface was rough and composed of stacked graphitic carbon layers whose size falls in the micrometer range. Several nanosized TiO_2 nanoparticles in aggregated forms were also observed on the surface. For better clarity, the N-TiO_2/C surface was visualized under higher magnifications, which clearly showed that the spherical-shaped TiO_2 nanoparticles are anchored on the surface of graphitic layer (Figure 2b). The average diameter of the spherical TiO_2 nanoparticles was measured using ImageJ software and it was found to be around 21.7 nm. Furthermore, TEM analysis of N-TiO_2/C was also performed and the images obtained at different magnifications are shown in Figure 2c−e. As seen in Figure 2c,d, the average interlayer distance measured between the lattice planes of TiO_2 was 0.247 nm. TEM micrographs also showed the dense agglomerated sheetlike structure with TiO_2 nanoparticles maintaining their spherical shape (Figure 2e). EDAX conducted for the sample ensured the presence of carbon, nitrogen, and titanium in the sample (Figure 2j). The scanning TEM (STEM) image (Figure 2f) with corresponding elemental mapping further confirmed the presence of graphitic carbon (Figure 2g), nitrogen (Figure 2h), and titanium (Figure 2i) in N-TiO_2/C.

To determine the crystal structure of N-TiO_2/C, powder X-ray diffraction (XRD) was conducted and the experimental data are presented in Figure S1. N-TiO_2/C displayed diffraction peaks (2θ) at 25°, 38°, 48°, 53°, 55°, 63°, 69°, 71°, and 73°, which can be correlated with the (*hkl*) indices (101), (004), (200), (105), (211), (204), (116), (220), and (215) of anatase TiO_2, respectively.[24,32] The XRD pattern of N-TiO_2/C showed that the major peaks were identical in shape and peak position to that of standard anatase TiO_2. Because of the overlapping of adjacent (103), (004), and (112) diffraction peaks, a broadened diffraction peak centered at around 42° was observed. This property is the indication that TiO_2 has nanometer particle size, which is one of the most influencing factors in determining the catalytic activity of any photocatalyst.[32] The formation of graphitic carbon was difficult to distinguish in the XRD patterns of N-TiO_2/C because of peak overlapping and widening. To further characterize the material, FT-IR was performed and the results are shown in Figure S2. In the spectrum of N-TiO_2/C, broad peaks belonging to C−N stretching bonds were observed in the region 1000−1300 cm^{-1}, which were not found in undoped TiO_2.[33] Similar peaks were present in the spectra of N doped carbonaceous (N-C) material. The results indicated the formation of graphite C−N structures along with the growth of TiO_2 during the pyrolysis. The peak at around 500 cm^{-1} (Figure S2b,c) represented vibration of the Ti−O−Ti bond,[34] which was found in undoped TiO_2 and N-TiO_2/C but not in N-C materials.

To probe the elemental state, the N-TiO_2/C was characterized by XPS (Figure 3). The elemental compositions of C, N, Ti, and O atoms were examined from XPS survey scan

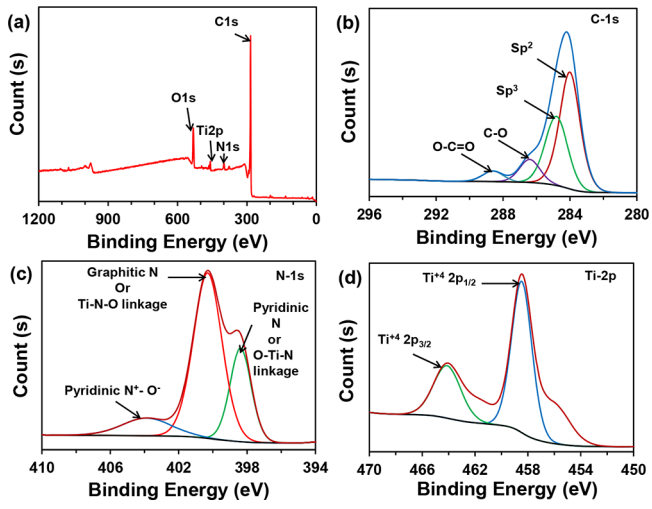

Figure 3. (a) Survey XPS spectrum and narrow scans of (b) C 1s, (c) N 1s, and (d) Ti 2p, XPS spectra of the N-TiO_2/C.

DOI: 10.1021/acsomega.8b01020
ACS Omega 2018, 3, 8111−8121

(Figure 3a) with their characteristic peaks centered at around 284.00, 400.00, 459.00, and 532.00 eV, respectively. The contents of C, N, Ti, and O in N-TiO_2/C were found to be 82.2, 3.6, 11.5, and 1.1%, respectively (Table S1). The narrow scan C 1s spectrum (Figure 3b) reveals that it was resolved into four different peaks with binding energies of 284.00, 284.80, 286.58, and 288.78 eV, which were attributed to sp^2 carbon, sp^3 carbon, carbon with hydroxy or ethers (C−OH, C−O−C), and carbonyl carbons (C═O), respectively. Figure 3c shows the narrow scan N 1s spectrum for N-TiO_2/C, which were fitted with three peaks at about 398.48, 400.48, and 404.08 eV, corresponding to pyridinic N, graphitic N, and pyridinic N^+-O^-, respectively.[35] However, in some literature studies, it was noted that the peak at 398.48 eV might be attributed to the N bonded in O−Ti−N linkage.[36−38] The peak at 400.48 eV might be due to the presence of N in the Ti−N−O environment.[36] Therefore, the broad peak at 398.38 eV could be due to both pyridinic N and O−Ti−N linkage N, and another broad peak at 400.48 eV could be due to the mixture of both graphitic N and N in Ti−N−O linkage. The narrow scan Ti 2p spectrum is shown in Figure 3d. The spectrum can be fitted with two peaks at 458.68 and 464.28 eV corresponding to the N-doped TiO_2 containing Ti^{4+} ($2p_{1/2}$) and Ti^{4+} ($2p_{3/2}$), respectively. The decrease in binding energy of pure TiO_2 from 459.54 to 458.68 eV is due to the N-doping to TiO_2.[18]

The amount of TiO_2 present in N-TiO_2/C was more precisely estimated by performing TGA of the N-TiO_2/C catalyst. TGA of the sample was performed three times using an air flow rate of 50 mL min^{-1} and a heating ramp of 5 °C min^{-1} up to 850 °C to get the more accuracy of the data. TGA curve (Figure S3a) shows the initial weight loss of 4% from room temperature to 150 °C, which was assigned to physically adsorbed water. The pronounced second weight loss of 64% from 330 to 530 °C was attributed to the decomposition of nitrogen-doped carbonaceous material. The residual material remaining after 850 °C was 30% of initial total weight of the sample, which was attributed to TiO_2. Additionally, the residual material was further tested by EDAX (Figure S3b) to confirm the presence of TiO_2. The EDAX spectrum shows that most of the residual sample was TiO_2. The inset SEM image of residual material showed the presence of crystalline needlelike structure of TiO_2. Furthermore, the surface area and porosity of N-TiO_2/C were determined using BET analysis. The BET linear isotherm plot for adsorption/desorption cycle (Figure S4a) and Barrett, Joyner and Halenda (BJH) pore size distribution plot (Figure S4b) proved the presence of abundant micropores along with some mesopores. The BET surface area and BJH average pore volume of N-TiO_2/C were found to be 21.97 m^2/g and 0.024 cm^3/g, respectively, which enhanced the adsorption of NPs and aided for their degradation.

To study the photocatalytic efficacy of N-TiO_2/C, 4-NP was chosen for the detailed photodegradation study. All other NPs were studied under the similar conditions. Before testing the degradation of 4-NP in the presence of visible light, various control studies were performed in the presence and absence of UV light as shown in Figure S5. It can be observed that using N-TiO_2/C, 85% of 4-NP was degraded in the presence of UV light compared to 10% removal in the absence of UV light after 150 min of treatment. For the control study, the effect of UV light without N-TiO_2/C, anatase TiO_2, and N-C was tested separately on the degradation of 4-NP. In the absence of N-TiO_2/C, UV light alone could not degrade 4-NP. The result clarified the fact that the presence of catalyst was essential for the degradation of NPs. Similarly, the difference in the percentage degradation of 4-NP (25%) using N-TiO_2/C and anatase TiO_2 under similar conditions indicated that the doping of N on carbon played a significant role in the degradation of 4-NP. Furthermore, the role of N-doped TiO_2 in N-TiO_2/C for 4-NP degradation is also shown in Figure S5. The presence of N-doped TiO_2 showed better performance for the 4-NP degradation. 4-NP was degraded more efficiently using the N-TiO_2/C sample (85%) compared to N-C sample (26%) after 150 min of UV light exposure. After analyzing the data, it was confirmed that the N-TiO_2/C was photocatalytically active and an efficient catalyst.

However, the use of UV light can be costly and physically hazardous.[39] Therefore, we evaluated the degradation of NPs in the presence of less expensive and harmless visible light. Figure 4a represents the efficacy of N-TiO_2/C for the

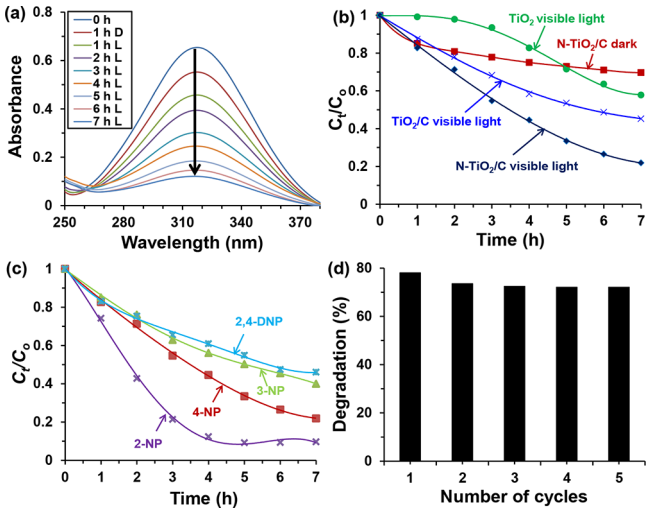

Figure 4. (a) UV−vis spectrum of 4-NP degradation in the presence of visible light, (b) control study for the 4-NP degradation, (c) comparative study of different NPs degradation, and (d) recyclability test of N-TiO_2/C for the degradation of 4-NP after 7 h of reaction. Experimental conditions: 10 mg L^{-1} NPs solution at pH 3, 20 mg of N-TiO_2/C at room temperature. *"D" stands for "dark" and "L" stands for "light".

degradation of 4-NP under visible light. Additionally, the control studies were performed (Figure 4b) for the comparison of 4-NP degradation under different conditions using (i) TiO_2 in the presence of visible light, (ii) TiO_2 and carbon nanocomposite (TiO_2/C) in the presence of visible light, and (ii) N-TiO_2/C in the absence of visible light. After 7 h, 80% of 4-NP with an initial concentration of 10 mg L^{-1} was degraded in the presence of N-TiO_2/C under visible light. In the absence of visible light, N-TiO_2/C removed only 30% of the 4-NP under similar conditions. It also confirmed that N-TiO_2/C was porous in nature. It was also observed that TiO_2/C removed 54% of 4-NP under similar reaction conditions. The noticeable difference (26%) for the degradation of 4-NP using N-TiO_2/C material compared to TiO_2/C was due to the effect of possible N-doping in the N-TiO_2/C material. As the control experiment showed that TiO_2 alone as the catalyst degraded only 42% of 4-NP after 7 h of reaction. When TiO_2 alone was used to degrade 4-NP, the degradation rate was

DOI: 10.1021/acsomega.8b01020
ACS Omega 2018, 3, 8111−8121

found to be slow initially. However, after 3 h of visible light exposure, the degradation profile was similar to that of the N-TiO_2/C catalyst. The similar degradation profile indirectly verifies the possible role of N-doped TiO_2 for degradation of 4-NP. Additionally, the photocatalytic activity of N-TiO_2/C material was extended by performing an experiment for the degradation of 2-chlorophenol (2-CP) (Figure S6) under similar conditions. After 5 h of visible light irradiation, 88% of 2-CP was degraded whereas only 66% 4-NP degradation was obtained under similar conditions. The faster degradation of 2-CP was attributed to the electron donating and withdrawing effect of chlorine, which activates the benzene ring and facilitates the degradation process.[40,41] The excellent photocatalytic activity of N-TiO_2/C under visible light may be attributed to the fact that during synthesis TiO_2 interacts strongly with the hydroxyl groups of nanostructured NCs in the presence of polydopamine, which results in more doping on N-TiO_2/C and generation of spherically shaped anchored TiO_2 on the surface of graphitic carbonaceous structures. Because of the formation of such structures, it is possible to produce close intimate interfacial interactions between TiO_2 at 2D heterojunction of the layers. As a result of this, the charge separation process during photocatalysis may become easier which aid in the overall photocatalytic activity by N-TiO_2/C.[26] We have recently synthesized a similar carbonaceous material involving TiO_2 and polydopamine (NGC-TiO_2). However microcrystalline cellulose was used for the synthesis. In this material, TiO_2 nanoparticles were found embedded inside the graphitic carbon layers. Because of this, NGC-TiO_2 suppressed desire photocatalytic activity but showed adsorption behavior.[42] Therefore, another reason for the enhanced photocatalytic activity under visible light could be attributed to the sufficient adsorption of 4-NP on the surface of N-TiO_2/C.

The pH of the medium is an important factor in catalysis because it determines the interaction between the catalyst and organic impurities.[43] Therefore, optimized pH of the NP containing solution is necessary for the effective degradation of NP in the presence of a catalyst. Solution pH ranging from 2 to 10 was selected for the optimization. The effect of solution pH on 4-NP degradation in the presence of visible light is shown in Figure S7. It was observed that the degradation rate increased with increasing pH up to 3 and then decreased with further increasing the solution pH. The optimized pH for 4-NP degradation was found to be 3. 4-NP undergoes dissociation to the phenolate ion if the pH of the solution is greater than its pK_a (7.15) value.[44] In acidic pH (pH < 7), 4-NP remains in a molecular form. The pH of the solution affects the surface charge of the catalyst and consequently adsorption and degradation of the organic pollutants.[45,46] In acidic solution, the surface of the N-TiO_2/C is most likely to be positively charged because of the protonation of any pyridinic N present in the catalyst. The point of zero charge (PZC) might be another reason for catalyst being positively charged.[47,48] The pH_{PZC} of the TiO_2 is reported in the range of 6.25−6.90. Because TiO_2 was used for the synthesis, we assume that pH_{PZC} of NTiO_2/C is also in the similar range. Therefore, the surface of the catalyst becomes positively charged if pH < pH_{PZC} and negatively charged pH > pH_{PZC} as shown in eqs 1 and 2.[48]

$$pH < pH_{PZC}: TiOH + H^+ = TiOH_2^+ \quad (1)$$

$$pH > pH_{PZC}: TiOH + OH^- = TiO^- + H_2O \quad (2)$$

In the acidic pH solution, electrostatic interaction between the positively charged surface of the catalyst and the lone pairs of electron present on the nitrogen and oxygen atoms of 4-NP brings molecular 4-NP more closely to the surface of the catalyst, which results in higher degradation.[49] However, if the pH < 3, the percentage degradation of 4-NP diminished. In this condition, $^{\bullet}OH$ radical produced on the surface of the catalyst may interact with Cl^- (due to the addition of strong HCl solution) to produce the $^{\bullet}OCl$ radical which is less reactive than $^{\bullet}OH$.[47] Another possible reason for decreasing degradation efficiency of the catalyst at pH < 3 is due to the repulsion between partially protonated lone pair of electrons of phenolic oxygen atom of 4-NP and positively charged surface of the catalyst.[49] In alkaline pH (pH > 7), negative charges are developed on the surface of the catalyst and the phenolate ion formed after the dissociation of 4-NP is repelled from the catalyst surface.[50] This reduces the proximity of 4-NP with the reactive oxygen species generated on the surface of the catalyst and decreases the overall degradation.

The photocatalytic efficacy of N-TiO_2/C was tested for the degradation of different NPs as well. 2-NP, 3-NP, 4-NP, and 2,4-dinitrophenol (2,4-DNP) were tested for degradation under similar optimized conditions. The decrease in the concentration of NP in the solution was evaluated by measuring the change in absorbance peak at their corresponding λ_{max}. Figure 4c illustrates the decrease in concentration of different NPs with time using N-TiO_2/C under visible light condition. The results exhibit that 2-NP was degraded more efficiently compared to other NPs. The degradation efficiency of N-TiO_2/C reached 90% in case of 2-NP compared to 80% for 4-NP, 60% for 3-NP, and 54% for 2,4-DNP in the presence of visible light after 7 h of reaction at room temperature. The results were in agreement with those reported by Kavitha and Palanivelu,[39] which explained that the position and numbers of $-NO_2$ group in the phenolic compound affect the ability of their degradation on the surface of the catalyst. They also reported that the $^{\bullet}OH$ undergoes electrophilic attack on ortho and para positions of phenolic −OH groups with more preferably to the para position. Therefore, 2-NP being electron-rich in the para position degraded faster than 4-NP being electron-rich in the ortho position. On the other hand, $-NO_2$ group are ortho- and para-deactivating group.[14] Therefore, 3-NP was difficult to degrade under similar conditions. In addition to the deactivating effect of $-NO_2$ group, the presence of two $-NO_2$ groups in 2,4-DNP blocks the favorable positions susceptible to $^{\bullet}OH$ attack. This is the reason for the less degradation of 2,4-DNP under similar conditions. On the other hand, the effect of $O_2^{\bullet-}$ radical for NPs degradation cannot be neglected. According to the report of Hameed et al.,[51] the proper orientation of $-NO_2$ group in 2-NP creates soft site for $O_2^{\bullet-}$ radical attack on the benzene ring. In 4-NP, the presence of additional negative inductive effect prevents the approach of $O_2^{\bullet-}$, resulting in less degradation compared to 2-NP. In case of 3-NP, the improper position (meta-position) of $-NO_2$ group causes less degradation. Similarly, in case of 2,4-DNP, the presence of bulkier $-NO_2$ group hinders the sites for attack by $O_2^{\bullet-}$ radical.

In terms of economy, the stability and reusability of the catalyst are crucial factors for the removal of organic pollutants. Multiple use of the catalyst remarkably minimizes the cost of the water purification. In the present work, the catalyst was used for five different cycles for 4-NP degradation as shown in Figure 4d. The recyclability experiment was performed in the

DOI: 10.1021/acsomega.8b01020
ACS Omega 2018, 3, 8111−8121

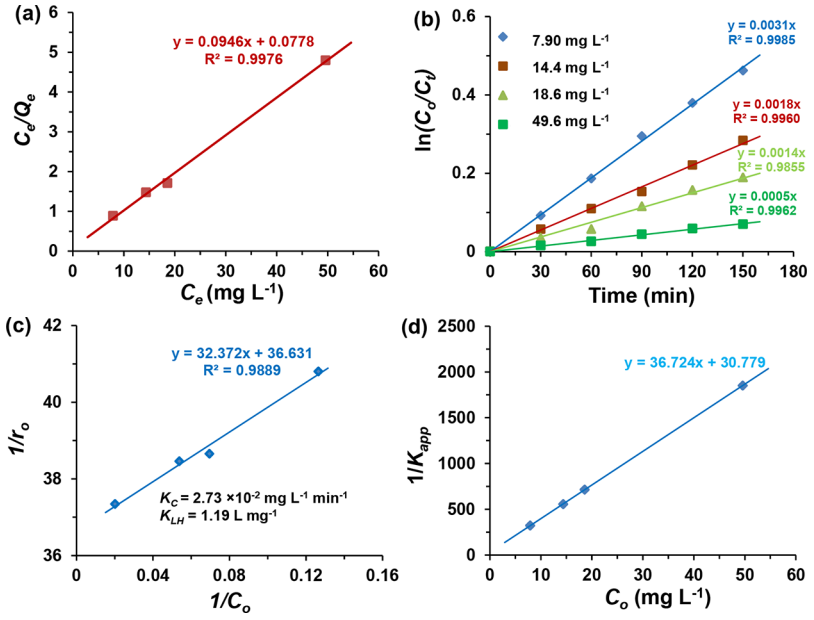

Figure 5. Linear plots of (a) C_e/Q_e vs C_e based on the Langmuir monolayer adsorption model, (b) $\ln(C_o/C_t)$ vs time for different initial 4-NP concentrations, (c) $1/r_o$ vs $1/C_o$, and (d) $1/K_{app}$ vs C_o based on the L−H kinetic model. Experimental conditions: 4-NP solution at pH 3, 20 mg of N-TiO_2/C at room temperature.

presence of visible light under optimized conditions. After each cycle of photocatalytic degradation, the catalyst was recovered by centrifuging and repeated washing with methanol and doubly distilled deionized (DI) water to remove the adsorbed 4-NP or its degraded products. The regenerated catalyst was dried completely and used for the next identical batch experiments. The results indicated that the N-TiO_2/C was efficient to remove 4-NP. In the 1st cycle, 80% of the 4-NP solution was degraded after 7 h of reaction. The percentage of 4-NP degradation remained almost consistent in the subsequent cycles. The slight decrease in the percentage degradation of 4-NP in the subsequent cycles might be due to the loss of sample during the washing process.

Degradation of organic pollutants was initiated by the reactive species such as $^{\bullet}OH$ or $O_2^{\bullet-}$ present on the surface of the catalyst. For the effective degradation of the organic pollutants, the proximity of the oxidizing species should be necessary.[39] Therefore, the adsorption of organic pollutants on the surface of catalyst will influence their degradation rate under light illumination. To study the adsorption behavior of 4-NP on the surface of N-TiO_2/C, a Langmuir adsorption model was fitted and the adsorption constant under the equilibrium condition was calculated using eq 3.[52]

$$\frac{C_e}{Q_e} = \frac{1}{(K_{ads} \times Q_m)} + \frac{C_e}{Q_m} \tag{3}$$

where C_e (mg L^{-1}) is the equilibrium concentration; K_{ads} (L mg^{-1}) is the Langmuir adsorption constant; Q_e (mg g^{-1}) is the adsorbed equilibrium quantity, and Q_m (mg g^{-1}) is the maximum adsorbed quantity. Q_m and K_{ads} can be calculated from the slope and intercept of the straight line, respectively, using the plot of C_e/Q_e versus C_e. The 4-different initial 4-NP concentrations of 10, 15, 20, and 50 mg L^{-1} were taken to study the dark adsorption kinetics. Using the eq 3, the linear plot of C_e/Q_e against C_e was drawn as shown in Figure 5a and the values of K_{ads} and Q_m were determined as 1.22 L mg^{-1} and 10.57 mg g^{-1}, respectively.

For the kinetic study of the photocatalytic degradation of 4-NP, four different initial 4-NP concentrations of 7.90, 14.4, 18.6, and 49.6 mg L^{-1} obtained after 1 h of 4-NP adsorption in the dark were considered in this batch experiment. Figure 5b shows the linear plot of $\ln(C_o/C_t)$ versus time with different initial concentrations of 4-NP solution. The 4-NP degradation followed the pseudo-first-order kinetic given in the following eq 4 as

$$\ln\left(\frac{C_o}{C_t}\right) = k_{app}t \tag{4}$$

where k_{app} (min^{-1}) is the apparent pseudo-first-order reaction rate constant. Also, C_o and C_t are 4-NP concentrations (mg L^{-1}) at the initial and at time t, respectively. The k_{app} values for four different initial concentrations of 4-NP were obtained directly from the regression analysis of the linear curve present in Figure 5b. The k_{app} values along with initial rates of reaction are given in Table S2. It was observed that the degradation rate constant values decreased with the increase in the initial 4-NP concentrations. To examine the effect of the initial 4-NP concentration on the reaction rate, a Langmuir−Hinshelwood (L−H) adsorption model was applied. The L−H adsorption model[52−54] can be expressed in the following eq 5 as

$$r_o = k_{app}C_o = \frac{K_C K_{LH} C_o}{1 + K_{LH} C_o} \tag{5}$$

where r_o (mg L^{-1} min^{-1}) is the initial rate of photocatalytic degradation of 4-NP, k_{app} (min^{-1}) is the apparent rate constant, K_{LH} (L mg^{-1}) is the L−H adsorption constant, and k_C (mg L^{-1} min^{-1}) is the L−H rate constant of the surface reaction, respectively. The linear form of the L−H adsorption model can be expressed as shown in following eq 6.

$$\frac{1}{r_o} = \frac{1}{k_C} + \frac{1}{k_C K_{LH}}\left(\frac{1}{C_o}\right) \tag{6}$$

DOI: 10.1021/acsomega.8b01020
ACS Omega 2018, 3, 8111−8121

The linear plot of $1/r_o$ against $1/C_o$ as shown in Figure 5c gives the linear relationship between $1/r_o$ and $1/C_o$. From the value of intercept $(1/k_C)$ and slope $(1/k_C K_{LH})$, k_C and K_{LH} values were determined to be 2.73×10^{-2} mg L^{-1} min^{-1} and 1.13 L mg^{-1}, respectively.

Equation 5 can also be rearranged to obtain the following eq 7, which gives the linear relationship of $1/K_{app}$ and C_o as shown in the Figure 5d.

$$\frac{1}{K_{app}} = \frac{1}{K_C K_{LH}} + \frac{C_o}{K_C} \quad (7)$$

The linear plot of $1/K_{app}$ versus C_o gave the straight line with the slope of $1/K_C$ and intercept of $1/K_C K_{LH}$. From the slope and intercept, the values of K_C and K_{LH} were calculated to be the same as obtained above from the plot of $1/r_o$ against $1/C_o$.

The constant values obtained from the L−H adsorption model and the Langmuir adsorption isotherm model were found to be close to each other (K_{ads} = 1.08K_{LH}). This result confirmed that photocatalytic degradation of 4-NP at pH 3 followed the L−H model satisfactorily under visible light.[55]

We believe that during the visible light irradiation of 4-NP in the presence of N-TiO_2/C, a number of intermediate products were formed, which were finally mineralized into inorganic products such as CO_2, CO, and H_2O. To detect the possible compounds formed during the reaction, we used gas chromatography−mass spectrometry (GC/MS), FT-IR, ion-chromatography (IC), and total organic carbon (TOC) analysis. At first, the intermediate products obtained after the degradation of 4-NP were detected by GC/MS analysis. Table 1 shows the list of intermediate products of 4-NP after degradation along with their formula, molecular mass, and the retention time in the gas chromatogram. As it can be seen in Table 1, many of the products are acids and alcohols and they are produced in low concentrations. Particularly, acids and more polar intermediates with high molecular mass are difficult to detect in GC/MS without derivatization. Therefore, after the reaction, the products were extracted in an organic solvent (ethyl acetate) and then reacted with bis(trimethylsilyl)-trifluroacetamide (BTSTFA) (a silylating agent) to make them volatile for facile detection in GC/MS. The GC chromatogram of 4-NP degradation with some intermediate products are shown in Figure S8 and mass spectra of some of the trimethylsilyl (TMS) derivative of intermediate products are shown in Figures S9 and S10. The major intermediate products detected after 30 min of 4-NP degradation include low molecular weight alcohols such as isobutanol, 1,3-propendiol, and glycerol with their retention times of 3.41, 11.33 and 18.41 min, respectively. Smaller acids such as formic acid, acetic acid, oxalic acid, and lactic acid with their corresponding retention times of 1.23, 2.73, 6.69, and 11.91 min, respectively, were also detected during the degradation (Figure S8). These intermediate products further degraded to give CO_2, CO, and H_2O.

Table 1. List of 4-NP Degraded Intermediate Products Obtained from the GC/MS Study[a]

name of intermediate products	retention time (min)	molecular weight (g mol^{-1})	molecular formula
formic acid	1.23	46	CH_2O_2
acetic acid	2.73	60	$C_2H_4O_2$
isobutanol	3.41	74	$C_4H_{10}O$
oxalic acid	6.69	90	$C_2H_2O_4$
2-methyl-1-butanol	7.43	88	$C_5H_{12}O$
1,3-propendiol	11.33	76	$C_3H_8O_2$
lactic acid	11.91	90	$C_3H_6O_3$
hydroquinone	16.99	110	$C_6H_6O_2$
glycerol	18.41	92	$C_3H_8O_3$

[a]All of the above compounds are TMS derivative of intermediate products.

The mechanism of 4-NP degradation is still not fully understood in general. The possible mode of 4-NP degradation initiated by reactive oxygen species such as $^{\bullet}OH$ and $O_2^{\bullet-}$ radicals is schematically represented in Figure S11. $^{\bullet}OH$ being a neutral radical and having similar reactivity as of $^{\bullet}F$ initiates the degradation of 4-NP forming different aromatic intermediates.[56] On the other hand, the $O_2^{\bullet-}$ radical bearing free radical along with an additional negative charge initiates the degradation reaction by attacking and cleaving the aromatic benzene ring to furnish directly aliphatic intermediates without forming any aromatic intermediates.[51] No aromatic intermediate products such as *p*-nitrocatechol, 4-nitropyrogallol, 1,2,4-trihydoxybenzene, and so forth other than hydroquinone were detected in the GC/MS analysis. The possible reason might be either due to the rapid degradation of these intermediate products into smaller aliphatic intermediates or inability to be detected in GC/MS because of their high molecular weight. Furthermore, the aliphatic intermediate products might be formed quickly by the attack of $O_2^{\bullet-}$ radical to give the nitrite ion, which can be further oxidized to the nitrate ion.[51] The aliphatic intermediates were further attacked by the $O_2^{\bullet-}$ or $^{\bullet}OH$ radical to produce mineralized products.

Additional information on the mineralization of 4-NP was obtained from TOC and IC analyses. From the TOC result, it was confirmed that 4-NP was degraded to smaller fragments such as CO and CO_2. Before degradation, the theoretical TOC value for 4-NP was calculated to be 5.2 mg L^{-1} (for 10 mg L^{-1} of 4-NP), which changed to 1.7 mg L^{-1} after 7 h of reaction with N-TiO_2/C in the presence of visible light. The result showed that 67% of 4-NP was mineralized into species such as CO_2 and CO. We believe some intermediates (e.g., acetic acid), which formed after degradation of 4-NP, are recalcitrant and remained for a longer time without further degradation.[57] Therefore, percentage of TOC removal was found to be less as compared to the percentage degradation of 4-NP, which was earlier estimated by UV−vis analysis. The TOC removal percentage achieved using N-TiO_2/C was higher than TOC removal efficiency (42%) by radiation-induced degradation of 4-NP using TiO_2.[58] Wang et al. reported the activity of the TiO_2 nanocomposite for degradation of 4-NP, where 47% decrease of TOC was observed after 400 min.[59] This is much lower than the TOC efficiency that was achieved in 420 min using N-TiO_2/C. In some cases, higher TOC removal of 4-NP has been reported using doped TiO_2 catalyst but required a longer time (more than 7 h) of light irradiation and a high dose of the catalyst.[60] Similarly, the mineralization of 4-NP can be detected by measuring the concentration of ammonium and nitrate ions formed using the IC technique.[61] The theoretical concentrations of ammonium and nitrate ion in the 4-NP solution for the complete mineralization process were calculated to be 1.29 and 4.46 mg L^{-1} (for 10 mg L^{-1} of 4-NP), respectively. For the blank studies, their concentrations were found to be 0.1 and <0.05 mg L^{-1}, respectively. After 7 h of photocatalytic degradation of 4-NP, the concentration of mineralized products such as ammonium and nitrate ions

DOI: 10.1021/acsomega.8b01020
ACS Omega 2018, 3, 8111−8121

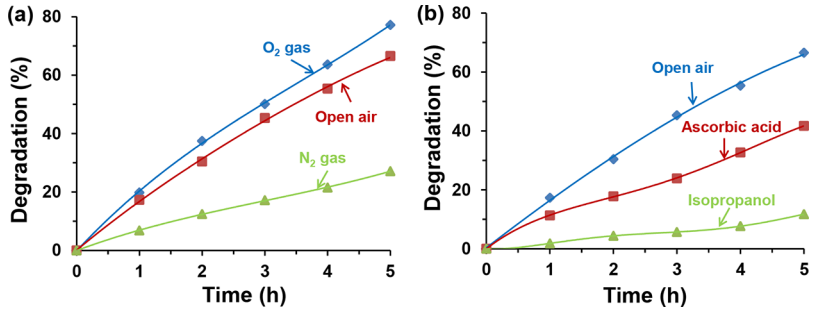

Figure 6. Effect of (a) oxygen and (b) radical quenchers on the percentage degradation of 4-NP solution in the presence of N-TiO_2/C under visible light. Experimental conditions: 10 mg L^{-1} 4-NP solution at pH 3, 20 mg of N-TiO_2/C at room temperature.

reached to 0.51 and 1.2 mg L^{-1}, respectively, exhibiting the 32 and 26% of mineralization into respective species. From the literature, it can be found that the ammonium ion takes time to oxidize into the nitrate ion.[62] During the degradation process, some of the N atoms of 4-NP are released as nitrogen (N_2) gas, while some other N atoms remain in the intermediate products.[60] Therefore, the percentage of mineralization into nitrate and ammonium ions was found to be lesser than the percentage of degradation. Total nitrogen percentage conversion in the form of nitrate and ammonium ion achieved is comparable to the previously reported study. However, in their study, TiO_2 was used along with other metal oxides containing expensive and rare metals.[60]

Further insights in the degradation mechanism can be gained by FT-IR analysis of the solids obtained before and after degradation of 4-NP at certain intervals of time using N-TiO_2/C under visible light irradiation. The changes in the FT-IR spectra before and after 4 and 7 h of degradations are depicted in Figure S12. The broad and intense peak at around 3400 cm^{-1} can be attributed to the phenolic OH stretching peak of 4-NP before degradation (Figure S12a). The OH stretching peak intensity decreased with increasing the irradiation time from 4 to 7 h (Figure S12b,c). The characteristic peaks of 4-NP as shown in Figure S10a at 1600 cm^{-1} (aromatic C═C stretching), 1400 cm^{-1} (asymmetric N═O stretching), 750−690 cm^{-1} (aromatic C−H bending), and 3070 cm^{-1} (aromatic C−H stretching) disappeared after 4 and 7 h of degradation as shown in Figure S12b,c, respectively. The formation of smaller acids after degradation of 4-NP was verified by the appearance of new peak at around 1700 cm^{-1} (Figure S12b,c). The peak at around 1700 cm^{-1} was due to the carboxylic C═O bond stretching. The sharp peak at 1070 cm^{-1} assigned (Figure S12a,b) to alcoholic C−O stretching was detected till 4 h of degradation, which became less intense after 7 h of degradation. The sharp characteristic peak at 1330 cm^{-1} assigned to stretching frequency of nitrate ion was clearly observed in Figure S12b,c. This also supported the fact of 4-NP mineralization into the nitrate ion.[63]

The oxygen species either in the form of $^{\bullet}OH$ or $O_2^{\bullet-}$ radicals, which were generated on the surface of the catalyst during the e−h transfer, play an important role in the degradation of NPs.[64] To verify that, the effect of the oxygen was studied and the results are depicted in Figure 6a. It was presumed that the dissolved oxygen may have a role in the generation of the reactive species and eventually degradation of NPs. When solution was purged and saturated with oxygen gas (O_2), 77% of 4-NP was degraded. On the other hand, only 27% degradation was detected when the solution was saturated with N_2 gas. The degradation occurred in the presence of N_2 gas was due to the presence of oxygen in water. This indicates that oxygen species played a significant role for the 4-NP degradation. From Figure 6a, it is evident that only 10% more degradation of 4-NP was observed in the case of O_2 saturated condition compared to open air condition. This finding indicates that oxygen required for 4-NP degradation was sufficient from open air, which is more economic and beneficial for waste treatment.

To further understand the generation of $^{\bullet}OH$ or $O_2^{\bullet-}$ radicals during the photocatalysis, radical quenching reactions were performed. Ascorbic acid, which is a quencher of $O_2^{\bullet-}$ radical, and isopropanol, an $^{\bullet}OH$ radical quencher, were used to indirectly detect the radicals and confirm their possible roles on degradation.[65,66] The concentration of quenchers used in the experiment was 10 times higher than the 4-NP concentration in the reaction mixture. From the Figure 6b, it is evident that the use of radical quenchers suppressed the degradation rate of 4-NP. After 5 h reaction, the catalyst alone was found to degrade only 67% of 4-NP. Isopropanol, on the other hand, showed a more retarding effect in the degradation. In the presence of isopropanol, only 12% 4-NP degradation was observed indicating the possible and major role of $^{\bullet}OH$ in the degradation. In the presence of ascorbic acid, N-TiO_2/C degraded 42% of 4-NP after 5 h of reaction. The less degradation observed in the presence of isopropanol compared to ascorbic acid might be due to the smaller size of isopropanol that might block the active sites by its adsorption along with the quenching effect. The results indicated that both radicals were found to be crucial for effective photocatalytic degradation of 4-NP.

CONCLUSIONS

In conclusion, photocatalytic degradation of NPs was successfully studied using N-TiO_2/C under visible light. The photocatalyst N-TiO_2/C was prepared by the sol−gel method followed by pyrolysis at 500 °C and characterized via SEM, TEM, EDAX, XRD, XPS, TGA, and BET techniques, which confirmed the N-doping in N-TiO_2/C nanocomposites. Photocatalytic activities of the material were tested by the degradation of 4-NP using visible and UV light. Acidic pH was found to be more suitable for 4-NP degradation with optimum pH of 3. Recyclability experiment showed that the N-TiO_2/C can be used multiple cycles without loss of activity. Photocatalytic efficacy of N-TiO_2/C was further extended by testing successful degradation of different NPs. The kinetic study revealed that the 4-NP degradation followed the pseudo-first-order kinetics. The K_{LH} and K_{ads} values obtained from the L−H adsorption kinetic model and the Langmuir adsorption

DOI: 10.1021/acsomega.8b01020
ACS Omega 2018, 3, 8111−8121

isotherm model, respectively, confirmed that the degradation study of 4-NP followed the L−H adsorption kinetic model satisfactorily. GC/MS and FT-IR studies confirmed that 4-NP degraded into smaller molecular fragments. TOC analysis showed that 67% of TOC in 4-NP mineralized into inorganic molecules such as CO_2 and CO after 7 h of reaction. Furthermore, IC analysis was performed to determine and confirm mineralization of 4-NP into less toxic products. Different radical quenchers were used to detect the possible role of reactive oxygen species in the photocatalytic degradation process. The synthesized NCs and dopamine-based catalyst has a promising potential for the degradation of other hazardous organic pollutants from wastewater.

EXPERIMENTAL SECTION

General. All chemicals were analytical grade reagents and were used as received without further purification. NCs (8 w/w %) was obtained from Blue Goose Biorefineries Inc. (Canada). Dopamine hydrochloride, anatase TiO_2 (size < 25 nm), 4-NP, 2,4-DNP, 2-CP, L-ascorbic acid, BTSTFA, potassium dihydrogen phosphate (KH_2PO_4), and dipotassium hydrogen phosphate (K_2HPO_4) were obtained from Sigma-Aldrich (USA). 2-NP and 3-NP were obtained from Acros Organics (USA). DI water was used to prepare all solutions. Ultrahigh purity N_2 and O_2 were obtained from NLR Welding Company, North Little Rock, Arkansas (USA). The details of the as-prepared N-TiO_2/C characterization instrumentations and techniques, the procedure for the degradation of NPs, and kinetic studies have been described in the Supporting Information.

Synthesis of the N-TiO_2/C Photocatalyst. N-TiO_2/C was synthesized by mixing NC, dopamine, and anatase TiO_2 in the ratio of 5:5:1 by weight in 25 mL of DI water and the mixture was stirred for 24 h in open air at room temperature. The pH of the mixture was maintained at 8 throughout the reaction. During this period, the reaction mixture turned black. After 24 h, the resulting mixture was filtered and the precipitate was washed with copious amounts of DI water. The residual black slurry was frozen at −20 °C and lyophilized using a Labconco FreeZone 1 L benchtop freeze dry system (Cole-Parmer, USA) to obtain a powdery black solid. The freeze-dried sample was then pyrolyzed at 500 °C using a tube furnace (model GSL-1100X, MTI Corporation, USA) for 2 h under continuous N_2 gas flow. The heating and cooling rates during pyrolysis were maintained at 10 °C min^{-1}. After pyrolysis, the sample was cooled to room temperature. Finally, a black carbonaceous material was obtained, which was further grounded into a fine powder using a mortar and pestle to generate N-TiO_2/C. The material was stored in a desiccator for further use. The synthesis of N-TiO_2/C is schematically represented in Figure 1b. N-C was synthesized following the same procedure but no TiO_2 was used during the synthesis. Similarly for the control experiment, TiO_2 and TiO_2/C material was synthesized using anatase TiO_2 and NCs. Additionally, anatase TiO_2 was treated at 500 °C for 2 h prior to use for any control reaction.

ASSOCIATED CONTENT

Supporting Information

The Supporting Information is available free of charge on the ACS Publications website at DOI: 10.1021/acsomega.8b01020.

Details of characterization techniques, photocatalytic studies and kinetics studies, degradation analyses, XRD of N-TiO_2/C; FT-IR of bare TiO_2, N-C, N-TiO_2/C; TGA of N-TiO_2/C; BET analysis of N-TiO_2/C; photocatalytic activity of N-TiO_2/C under UV light; comparative degradation study of 4-NP with 2-CP; effect of solution pH; GC chromatogram and MS spectra of 4-NP degraded intermediates; possible mechanism of 4-NP degradation; FT-IR of 4-NP degradation products; elemental analysis of N-TiO_2/C; and pseudo-first-order apparent rate constant (K_{app}) and initial rate of reaction (r_o) for 4-NP degradation (PDF)

AUTHOR INFORMATION

Corresponding Author

*E-mail: axghosh@ualr.edu. Phone: 501-569-8827. Fax: 501-569-8838 (A.G.).

ORCID

Jin-Woo Kim: 0000-0002-7119-8208

Anindya Ghosh: 0000-0002-6123-3209

Notes

The authors declare no competing financial interest.

ACKNOWLEDGMENTS

This research was financially supported by the National Science Foundation (grant no. IIA-1457888) and the Arkansas EPSCoR Program, ASSET III (CASE).

REFERENCES

(1) Mahy, J. G.; Tasseroul, L.; Zubiaur, A.; Geens, J.; Brisbois, M.; Herlitschke, M.; Hermann, R.; Heinrichs, B.; Lambert, S. D. Highly Dispersed Iron Xerogel Catalysts for P-Nitrophenol Degradation by Photo-Fenton Effects. *Microporous Mesoporous Mater.* **2014**, *197*, 164−173.

(2) Wu, D.; Tao, X.; Chen, Z.-P.; Han, J.-T.; Jia, W.-J.; Zhu, N.; Li, X.; Wang, Z.; He, Y.-X. The Environmental Endocrine Disruptor P-Nitrophenol Interacts with FKBP51, a Positive Regulator of Androgen Receptor and Inhibits Androgen Receptor Signaling in Human Cells. *J. Hazard. Mater.* **2016**, *307*, 193−201.

(3) Parida, K.; Das, D. P. Photo-Oxidation of 4-Nitrophenol in Aqueous Suspensions, Catalysed by Titania Intercalated Zirconium Phosphate (ZrP) and Titanium Phosphate (TiP). *J. Photochem. Photobiol. A* **2004**, *163*, 561−567.

(4) Kowalczyk, A.; Eyice, Ö.; Schäfer, H.; Price, O. R.; Finnegan, C. J.; van Egmond, R. A.; Shaw, L. J.; Barrett, G.; Bending, G. D. Characterization ofpara-Nitrophenol-Degrading Bacterial Communities in River Water by Using Functional Markers and Stable Isotope Probing. *Appl. Environ. Microbiol.* **2015**, *81*, 6890−6900.

(5) Min, J.; Wang, B.; Hu, X. Effect of Inoculation of Burkholderia Sp. Strain SJ98 on Bacterial Community Dynamics and Para-Nitrophenol, 3-Methyl-4-Nitrophenol, and 2-Chloro-4-Nitrophenol Degradation in Soil. *Sci. Rep.* **2017**, *7*, 5983.

(6) Hamidouche, S.; Bouras, O.; Zermane, F.; Cheknane, B.; Houari, M.; Debord, J.; Harel, M.; Bollinger, J.-C.; Baudu, M. Simultaneous Sorption of 4-Nitrophenol and 2-Nitrophenol on a Hybrid Geo-composite Based on Surfactant-Modified Pillared-Clay and Activated Carbon. *Chem. Eng. J.* **2015**, *279*, 964−972.

(7) Yao, Y.-X.; Li, H.-B.; Liu, J.-Y.; Tan, X.-L.; Yu, J.-G.; Peng, Z.-G. Removal and Adsorption ofp-Nitrophenol from Aqueous Solutions Using Carbon Nanotubes and Their Composites. *J. Nanomater.* **2014**, *2014*, 1−9.

(8) *Ambient Water Quality Criteria for Nitrophenols*; United States Environmental Protection Agency, Office of Water Regulations and Standards, Criteria and Standards Division: Washington, DC, 1980.

DOI: 10.1021/acsomega.8b01020
ACS Omega 2018, 3, 8111−8121

(9) Tewari, B. B. Removal of P-Aminophenol and P-Nitrophenol from Aqueous Solution through Adsorption on Bismuth, Lead, and Manganese Ferrocyanides and Their Relevance to Environmental Issues. *Russ. J. Phys. Chem. A* **2014**, *88*, 1564−1568.
(10) Tomei, M. C.; Annesini, M. C.; Prpich, G. P.; Daugulis, A. J. Biodegradation of 4-Nitrophenol in a Two-Phase System Operating with Polymers as the Partitioning Phase. *Environ. Sci. Technol.* **2009**, *43*, 7105−7110.
(11) Ayral, C.; Lebigue, C. J.; Stüber, F.; Wilhelm, A.-M.; Delmas, H. Catalytic Wet Air Oxidation of Phenolic Compounds and Mixtures over Activated Carbon: Conversion, Mineralization, and Catalyst Stability. *Ind. Eng. Chem. Res.* **2010**, *49*, 10707−10714.
(12) Chen, X.; Burda, C. The Electronic Origin of the Visible-Light Absorption Properties of C-, N- and S-Doped TiO_2 Nanomaterials. *J. Am. Chem. Soc.* **2008**, *130*, 5018−5019.
(13) Luc, W.; Jiao, F. Synthesis of Nanoporous Metals, Oxides, Carbides, and Sulfides: Beyond Nanocasting. *Acc. Chem. Res.* **2016**, *49*, 1351−1358.
(14) Priya, M. H.; Madras, G. Photocatalytic degradation of nitrobenzenes with combustion synthesized nano-TiO_2. *J. Photochem. Photobiol. A* **2006**, *178*, 1−7.
(15) Linsebigler, A. L.; Lu, G.; Yates, J. T. Photocatalysis on TiO_2 Surfaces: Principles, Mechanisms, and Selected Results. *Chem. Rev.* **1995**, *95*, 735−758.
(16) Kumar, S. G.; Devi, L. G. Review on Modified TiO_2 Photocatalysis under UV/Visible Light: Selected Results and Related Mechanisms on Interfacial Charge Carrier Transfer Dynamics. *J. Phys. Chem. A* **2011**, *115*, 13211−13241.
(17) Naraginti, S.; Stephen, F. B.; Radhakrishnan, A.; Sivakumar, A. Zirconium and silver co-doped TiO_2 nanoparticles as visible light catalyst for reduction of 4-nitrophenol, degradation of methyl orange and methylene blue. *Spectrochim. Acta, Part A* **2015**, *135*, 814−819.
(18) Nassoko, D.; Li, Y.-F.; Wang, H.; Li, J.-L.; Li, Y.-Z.; Yu, Y. Nitrogen-doped TiO_2 nanoparticles by using EDTA as nitrogen source and soft template: Simple preparation, mesoporous structure, and photocatalytic activity under visible light. *J. Alloys Compd.* **2012**, *540*, 228−235.
(19) Ansari, S. A.; Khan, M. M.; Ansari, M. O.; Cho, M. H. Nitrogen-doped titanium dioxide (N-doped TiO_2) for visible light photocatalysis. *New J. Chem.* **2016**, *40*, 3000−3009.
(20) Kaushik, B. K.; Majumder, M. K. *Carbon Nanotube Based VLSI Interconnects: Analysis and Design*, 1st ed.; Kaushik, B. K., Ed.; SpringerBriefs in Applied Sciences and Technology; Springer India: New Delhi, 2015; pp 1−14.
(21) Dong, H.; Zeng, G.; Tang, L.; Fan, C.; Zhang, C.; He, X.; He, Y. An overview on limitations of TiO_2-based particles for photocatalytic degradation of organic pollutants and the corresponding countermeasures. *Water Res.* **2015**, *79*, 128−146.
(22) Lee, W. J.; Lee, J. M.; Kochuveedu, S. T.; Han, T. H.; Jeong, H. Y.; Park, M.; Yun, J. M.; Kwon, J.; No, K.; Kim, D. H.; et al. Biomineralized N-Doped CNT/TiO_2 Core/Shell Nanowires for Visible Light Photocatalysis. *ACS Nano* **2012**, *6*, 935−943.
(23) Ong, W.-J.; Tan, L.-L.; Chai, S.-P.; Yong, S.-T.; Mohamed, A. R. Self-assembly of nitrogen-doped TiO_2 with exposed {001} facets on a graphene scaffold as photo-active hybrid nanostructures for reduction of carbon dioxide to methane. *Nano Res.* **2014**, *7*, 1528−1547.
(24) Zhang, Y.; Yang, H. M.; Park, S.-J. Synthesis and characterization of nitrogen-doped TiO_2 coatings on reduced graphene oxide for enhancing the visible light photocatalytic activity. *Curr. Appl. Phys.* **2018**, *18*, 163−169.
(25) Wayland, H. A.; Boury, S. N.; Chhetri, B. P.; Brandt, A.; Proskurnin, M. A.; Filichkina, V. A.; Zharov, V. P.; Biris, A. S.; Ghosh, A. Advanced Cellulosic Materials for Treatment and Detection of Industrial Contaminants in Wastewater. *ChemistrySelect* **2016**, *1*, 4472−4488.
(26) Lin, N.; Dufresne, A. Nanocellulose in Biomedicine: Current Status and Future Prospect. *Eur. Polym. J.* **2014**, *59*, 302−325.
(27) Henry, A.; Plumejeau, S.; Heux, L.; Louvain, N.; Monconduit, L.; Stievano, L.; Boury, B. Conversion of Nanocellulose Aerogel into TiO_2 and TiO_2@C Nano-thorns by Direct Anhydrous Mineralization with TiCl4. Evaluation of Electrochemical Properties in Li Batteries. *ACS Appl. Mater. Interfaces* **2015**, *7*, 14584−14592.
(28) Sinha, A.; Martin, E. M.; Lim, K.-T.; Carrier, D. J.; Han, H.; Zharov, V. P.; Kim, J.-W. Cellulose Nanocrystals as Advanced "Green" Materials for Biological and Biomedical Engineering. *J. Biosyst. Eng.* **2015**, *40*, 373−393.
(29) Kaushik, M.; Moores, A. Review: Nanocelluloses as Versatile Supports for Metal Nanoparticles and Their Applications in Catalysis. *Green Chem.* **2016**, *18*, 622−637.
(30) Liu, Y.; Ai, K.; Lu, L. Polydopamine and Its Derivative Materials: Synthesis and Promising Applications in Energy, Environmental, and Biomedical Fields. *Chem. Rev.* **2014**, *114*, 5057−5115.
(31) Dyke, J. C.; Hu, H.; Lee, D. J.; Ko, C.-C.; You, W. The Role of Temperature in Forming Sol-Gel Biocomposites Containing Polydopamine. *J. Mater. Chem. B* **2014**, *2*, 7704−7711.
(32) Liu, X.; Chen, N.; Li, Y.; Deng, D.; Xing, X.; Wang, Y. A General Nonaqueous Sol-Gel Route to G-C_3N_4-Coupling Photocatalysts: The Case of Z-Scheme G-C_3N_4/TiO_2 with Enhanced Photodegradation toward RhB under Visible-Light. *Sci. Rep.* **2016**, *6*, 39531.
(33) Zimmerman, J. L.; Williams, R.; Khabashesku, V. N.; Margrave, J. L. Synthesis of Spherical Carbon Nitride Nanostructures. *Nano Lett.* **2001**, *1*, 731−734.
(34) Chainarong, S.; Sikong, L.; Pavasupree, S.; Niyomwas, S. Synthesis and Characterization of Nitrogen-doped TiO_2 Nanomaterials for Photocatalytic Activities under Visible Light. *Energy Procedia* **2011**, *9*, 418−427.
(35) Wei, J.; Hu, Y.; Liang, Y.; Kong, B.; Zhang, J.; Song, J.; Bao, Q.; Simon, G. P.; Jiang, S. P.; Wang, H. Nitrogen-Doped Nanoporous Carbon/Graphene Nano-Sandwiches: Synthesis and Application for Efficient Oxygen Reduction. *Adv. Funct. Mater.* **2015**, *25*, 5768−5777.
(36) Sathish, M.; Viswanathan, B.; Viswanath, R. P. Characterization and photocatalytic activity of N-doped TiO_2 prepared by thermal decomposition of Ti-melamine complex. *Appl. Catal. B* **2007**, *74*, 307−312.
(37) Gole, J. L.; Stout, J. D.; Burda, C.; Lou, Y.; Chen, X. Highly Efficient Formation of Visible Light Tunable TiO_2-xNxPhotocatalysts and Their Transformation at the Nanoscale. *J. Phys. Chem. B* **2004**, *108*, 1230−1240.
(38) Li, H.; Li, J.; Huo, Y. Highly Active TiO_2N Photocatalysts Prepared by Treating TiO_2 Precursors in NH_3/Ethanol Fluid under Supercritical Conditions. *J. Phys. Chem. B* **2006**, *110*, 1559−1565.
(39) Kavitha, V.; Palanivelu, K. Degradation of Nitrophenols by Fenton and Photo-Fenton Processes. *J. Photochem. Photobiol. A* **2005**, *170*, 83−95.
(40) Hou, Y.; Yang, J.; Lei, C.; Yang, B.; Li, Z.; Xie, Y.; Zhang, X.; Lei, L.; Chen, J. Nitrogen Vacancy Structure Driven Photoeletrocatalytic Degradation of 4-Chlorophenol Using Porous Graphitic Carbon Nitride Nanosheets. *ACS Sustainable Chem. Eng.* **2018**, *6*, 6497−6506.
(41) Jawad, A.; Li, Y.; Guo, L.; Khan, A.; Chen, Z.; Wang, J.; Yang, J.; Liu, W.; Yin, G. Bimetallic synergistic degradation of chlorophenols by CuCoOx-LDH catalyst in bicarbonate-activated hydrogen peroxide system. *RSC Adv.* **2016**, *6*, 72643−72653.
(42) RanguMagar, A. B.; Chhetri, B. P.; Parnell, C. M.; Parameswaran-Thankam, A.; Watanabe, F.; Mustafa, T.; Biris, A. S.; Ghosh, A. Removal of Nitrophenols from Water Using Cellulose Derived Nitrogen Doped Graphitic Carbon Material Containing Titanium Dioxide. *Part. Sci. Technol.* **2018**, 1−9.
(43) Yang, L.; Luo, S.; Li, Y.; Xiao, Y.; Kang, Q.; Cai, Q. High Efficient Photocatalytic Degradation of p-Nitrophenol on a Unique Cu_2O/TiO_2 p-n Heterojunction Network Catalyst. *Environ. Sci. Technol.* **2010**, *44*, 7641−7646.
(44) Tasseroul, L.; Pirard, S. L.; Lambert, S. D.; Páez, C. A.; Poelman, D.; Pirard, J.-P.; Heinrichs, B. Kinetic study of p-

DOI: 10.1021/acsomega.8b01020
ACS Omega 2018, 3, 8111−8121

nitrophenol photodegradation with modified TiO_2 xerogels. *Chem. Eng. J.* **2012**, *191*, 441−450.
(45) Schneider, J.; Matsuoka, M.; Takeuchi, M.; Zhang, J.; Horiuchi, Y.; Anpo, M.; Bahnemann, D. W. Understanding TiO_2 Photocatalysis: Mechanisms and Materials. *Chem. Rev.* **2014**, *114*, 9919−9986.
(46) Shokri, A.; Mahanpoor, K.; Soodbar, D. Evaluation of a modified TiO_2 (GO B TiO_2) photo catalyst for degradation of 4-nitrophenol in petrochemical wastewater by response surface methodology based on the central composite design. *J. Environ. Chem. Eng.* **2016**, *4*, 585−598.
(47) Nezamzadeh-Ejhieh, A.; Khorsandi, S. Photocatalytic Degradation of 4-Nitrophenol with ZnO Supported Nano-Clinoptilolite Zeolite. *J. Ind. Eng. Chem.* **2014**, *20*, 937−946.
(48) Sun, J.; Qiao, L.; Sun, S.; Wang, G. Photocatalytic degradation of Orange G on nitrogen-doped TiO_2 catalysts under visible light and sunlight irradiation. *J. Hazard. Mater.* **2008**, *155*, 312−319.
(49) Nezamzadeh-Ejhieh, A.; Khodabakhshi-Chermahini, F. Incorporated ZnO onto Nano Clinoptilolite Particles as the Active Centers in the Photodegradation of Phenylhydrazine. *J. Ind. Eng. Chem.* **2014**, *20*, 695−704.
(50) J, A. I.; A, N. M. A Study on Removal Characteristics of Para-Nitrophenol from Aqueous Solution by Fly Ash. *J. Environ. Chem. Ecotoxicol.* **2011**, *3*, 32−36.
(51) Hameed, A.; Aslam, M.; Ismail, I. M. I.; Chandrasekaran, S.; Kadi, M. W.; Gondal, M. A. Sunlight assisted photocatalytic mineralization of nitrophenol isomers over W^{6+} impregnated ZnO. *Appl. Catal., B* **2014**, *160−161*, 227−239.
(52) Khezrianjoo, S.; Revanasiddappa, H. Langmuir-Hinshelwood Kinetic Expression for the Photocatalytic Degradation of Metanil Yellow Aqueous Solutions by ZnO Catalyst. *Chem. Sci. J.* **2012**, *CSJ-85*, 1−7.
(53) Barka, N.; Assabbane, A.; Nounah, A.; Ichou, Y. A. Photocatalytic degradation of indigo carmine in aqueous solution by TiO_2-coated non-woven fibres. *J. Hazard. Mater.* **2008**, *152*, 1054−1059.
(54) Chhetri, B. P.; Soni, D.; RanguMagar, A. B.; Parnell, C. M.; Wayland, H.; Watanabe, F.; Kannarpady, G.; Biris, A. S.; Ghosh, A. Synthesis, Characterization, and Photocatalytic Activity of N-Doped Carbonaceous Material Derived from Cellulose in Textile Dye Remediation. *J. Environ. Chem. Eng.* **2017**, *5*, 2586−2596.
(55) Guettaï, N.; Ait Amar, H. Photocatalytic Oxidation of Methyl Orange in Presence of Titanium Dioxide in Aqueous Suspension. Part II: Kinetics Study. *Desalination* **2005**, *185*, 439−448.
(56) Yu, S.; Hu, J.; Wang, J. Gamma radiation-induced degradation of p-nitrophenol (PNP) in the presence of hydrogen peroxide (H_2O_2) in aqueous solution. *J. Hazard. Mater.* **2010**, *177*, 1061−1067.
(57) Vautier, M.; Guillard, C.; Herrmann, J.-M. Photocatalytic Degradation of Dyes in Water: Case Study of Indigo and of Indigo Carmine. *J. Catal.* **2001**, *201*, 46−59.
(58) Shaoqing, Y.; Jun, H.; Jianlong, W. Radiation-induced catalytic degradation of p-nitrophenol (PNP) in the presence of TiO_2 nanoparticles. *Radiat. Phys. Chem.* **2010**, *79*, 1039−1046.
(59) Wang, C.; Li, J.; Mele, G.; Yang, G.-M.; Zhang, F.-X.; Palmisano, L.; Vasapollo, G. Efficient degradation of 4-nitrophenol by using functionalized porphyrin-TiO_2 photocatalysts under visible irradiation. *Appl. Catal. B* **2007**, *76*, 218−226.
(60) Chu, Y. Y.; Qian, Y.; Wang, W. J.; Deng, X. L. A Dual-Cathode Electro-Fenton Oxidation Coupled with Anodic Oxidation System Used for 4-Nitrophenol Degradation. *J. Hazard. Mater.* **2012**, *199−200*, 179−185.
(61) Kavitha, V.; Palanivelu, K. Degradation of Nitrophenols by Fenton and Photo-Fenton Processes. *J. Photochem. Photobiol. A* **2005**, *170*, 83−95.
(62) Stylidi, M.; Kondarides, D. I.; Verykios, X. E. Visible light-induced photocatalytic degradation of Acid Orange 7 in aqueous TiO_2 suspensions. *Appl. Catal., B* **2004**, *47*, 189−201.
(63) Goebbert, D. J.; Garand, E.; Wende, T.; Bergmann, R.; Meijer, G.; Asmis, K. R.; Neumark, D. M. Infrared Spectroscopy of the Microhydrated Nitrate Ions $NO_3^-(H_2O)_{1-6}$. *J. Phys. Chem. A* **2009**, *113*, 7584−7592.
(64) Divband, B.; Khatamian, M.; Eslamian, G. R. K.; Darbandi, M. Synthesis of Ag/ZnO Nanostructures by Different Methods and Investigation of Their Photocatalytic Efficiency for 4-Nitrophenol Degradation. *Appl. Surf. Sci.* **2013**, *284*, 80−86.
(65) Wang, D.; Guo, L.; Zhen, Y.; Yue, L.; Xue, G.; Fu, F. AgBr quantum dots decorated mesoporous Bi_2WO_6 architectures with enhanced photocatalytic activities for methylene blue. *J. Mater. Chem. A* **2014**, *2*, 11716−11727.
(66) Nandi, A.; Chatterjee, I. B. Scavenging of Superoxide Radical by Ascorbic Acid. *J. Biosci.* **1987**, *11*, 435−441.

DOI: 10.1021/acsomega.8b01020
ACS Omega 2018, 3, 8111−8121